Preprints of the 21st IFAC World Congress (Virtual)
Berlin, Germany, July 12-17, 2020

LiDAR Based Obstacle detection for Snow Groomers

L. Onesto * **M. Corno** * **L. Franceschetti** * **E. Hokka** **
S. M. Savaresi *

* *Dipartimento di Elettronica Informazione e Bioingegneria, Politecnico di Milano, via G. Ponzio 34/5, 20133, Milan, Italy. Email:* {*luca.onesto, matteo.corno, luca.franceschetti, sergio.savaresi*}*@polimi.it.*
** *TTControl GmbH - Ensuring Reliable Networks FN: 246 710i, Handelsgericht Wien. Email: ensio.hokka@ttcontrol.com.*

Abstract: This paper presents an obstacle detection system for snow groomers. The system is based on a 2D solid-states LiDAR sensor mounted on the top of the cabin. The measurements describe the surrounding environment through an Occupancy Grid framework, which is extended for this particular case study. The proposed approach set the occupancy probability of the surrounding environment based on the expected height of the obstacle. The method is extensively analyzed through experimental test on a snow groomer.

Keywords: Robot navigation, Estimation Algorithms, Navigation system, Obstacle detection

1. INTRODUCTION

Advanced-driver assistance systems (ADAS) have been proved to improve safety in cars (see Ziebinski et al. (2016)). ADAS are either active and passive. Active ADAS are capable to change the vehicle motion, while passive ones only provide useful information to the driver.

The literature has mostly focused on the prevention of casualties for road traffic vehicles, while only limited interest has been paid to off-highway vehicles (see Gustafsson and Eriksson (2013)). Among them, snowy-environment vehicles are also interested by a less-established legislation concerning licensing, safety education and minimum age (see Vanlaar et al. (2015)). Even though, the popularity and the diffusion of these vehicles is rising (see Yanchar et al. (2012)), the open scientific and technical literature is rather scarce on ADAS for this class of vehicles. This is due to several factors: a smaller market and the fact that in most cases, solutions developed for road vehicles are also applicable to this minor class (see Corno et al. (2018)).

Considering the case of a snow groomer, this paper presents an obstacle-detection system to warn the driver about the presence of obstacles in its trajectory. A snow groomer is a tracked vehicle equipped with a front main blade and a rear tiller. The main task of this heavy-duty vehicle is to maintain ski slopes of ski resorts. Snow groomers usually operate during night time, after slope closing time, to avoid possible collisions with skiers.

To the best of the authors' knowledge, the only study of ADAS for this kind of vehicles is in Broggi and Fascioli (2002) and describes an artificial-vision algorithm. The system allows the vehicle to follow the preceding one, through the detection of track footprints based on an image processing approach.

Conversely, in this paper, we study the possibility of using the Occupancy Grid framework, that provides a probabilistic occupancy representation of the environment. The idea was first applied to snowy environments by Kukko et al. (2013). They use a 3D laser scanner to estimate the snow surface roughness. The point cloud of the sensor provides a clear representation of the surrounding environment. The 3D approach is accurate, but very computationally demanding. In this work, instead, the proposed approach creates a map of the surrounding environment based on a 2D solid-state LiDAR sensor. This technology consists in a single fixed beam light source that is diffused through the use of an appropriate optics. The output data can be easily managed by the on-board CPU, moreover they are more cost effective than 3D LiDARs.

The main contributions of this paper are:

- the usage of a 2D solid-state LiDAR sensor for snowy environment;
- the extension of the Occupancy Grid approach, where the occupancy probability is updated in function of the expected height of the obstacles.
- the experimental validation of the proposed approach focused on the detection of a person in 3 different positions, namely standing, crouched and laying down.

This paper is organized as follows: Section 3 introduces the concept of the Occupancy Grid, Section 2 presents the experimental layout, Section 4 describes the proposed obstacle-detection system, Section 5 shows the experimental results.

2. EXPERIMENTAL LAYOUT

Figure 1 shows the experimental layout considered in this paper. The snow groomer model is a Prinoth Leitwolf. The standard set of available sensors is composed of:

- An encoder mounted on the transmission system, which measures the mean velocity of the tracks.
- A 6 axis Inertial Measurement Units (IMU) installed in the vehicle cabin. In the following analysis, only the yaw rate ω_z will be considered.

Moreover, the vehicle is equipped with:

- A 2D solid-state LiDAR. The model is a Leddar Vu8 designed by LeddarTech (see Leddartech (2019)).
- A camera mounted next to the LiDAR sensor. The video is recorded at 30 frames per second and it provides a clear understanding of the surrounding environment. The video is used for validation.

All the signals are logged by a Linux-based Laptop, with a ROS environment, installed in the cabin.

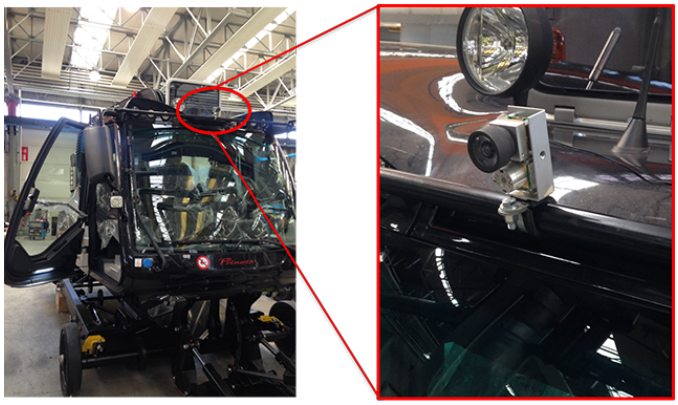

Fig. 1. Experimental Setup: Prinoth Leitwolf with the 2D LiDAR sensor mounted on the top of the cabin

The LiDAR sensor has an horizontal field of view (FOV) of 48 degrees which is divided in 8 sectors of the same size (8 degrees). Each sector provides the distance of the closest obstacle in its field of view. The sensor sampling time is 0.1 seconds. The measurement accuracy is 5 centimeters and the distance precision is 6 millimeters. The sensor range depends on the color and the reflectivity of the target: from 18 meters for grey targets with 18% of reflectivity to 31 meters for white targets with 90% of reflectivity, respectively.

3. OCCUPANCY GRID

This Section recalls the basic idea of the Occupancy Grid. An occupancy grid m is a discretized and probabilistic model of the environment. It is a spatial representation of the environment indicating the probability of each cell to be occupied by an obstacle. The probability is expressed by a random variable m_i where: $p(m_i) = 1$ if the cell is occupied, $p(m_i) = 0$ if the cell is free. The apriori probability for a cell for which no data is available is $p(m_i) = 0.5$. The general occupancy map problem can be casted into the Bayesian inference theory. In this framework, the problem of estimating the map m can be expressed by the posterior:

$$p(m|q_{1:t}, x_{1:t})$$

where $q_{1:t}$ and $x_{1:t}$ stand for the sensor measurements and the vehicle pose respectively from time instant 1 up to t. In Elfes (1989), the assumption of mutual independence between cells (indicated in what follows by a subscript) is introduced and heads to:

$$p(m|q_{1:t}, x_{1:t}) = \prod_i p(m_i|q_{1:t}, x_{1:t}). \tag{1}$$

The high dimensional mapping problem is decomposed into a collection of one dimensional problems (*i.e.* the occupancy of each grid cell is computed independently of others). Thrun et al. (2005) shows how (1) can be derived using Bayesian reasoning and introducing the hypothesis of *static environment* (*i.e.* there are no changes in the environment). The result is a recursive formula:

$$p(m_i|q_{1:t}, x_{1:t}) = \frac{1}{1 + \underbrace{f(m_i|q_t, x_t)}_{A} \cdot \underbrace{f(m_i|q_{1:t-1}, x_{1:t-1})}_{B} \cdot \underbrace{g(m_i)}_{C}} \tag{2}$$

where $f(m_i|q, x) = \frac{1-p(m_i|q,x)}{p(m_i|q,x)}$ and $g(m_i) = \frac{p(m_i)}{1-p(m_i)}$.

The following remarks are due:

- term A depends only on the last pose x_t and observation z_t. In particular, $p(m_i|q_t, x_t)$ is called *inverse sensor model* because it maps the latest sensor measurement back to its cause (*i.e.* the obstacle).
- term B is a recursive term and it depends on the previous poses and observations.
- term C stands for the prior knowledge of the map occupancy.

If there is no prior information on the environment, as in the case under analysis, the map is initialized to 0.5. In conclusion, the proposed algorithm iteratively updates the map exploiting the last pose x_t and the last observation q_t.

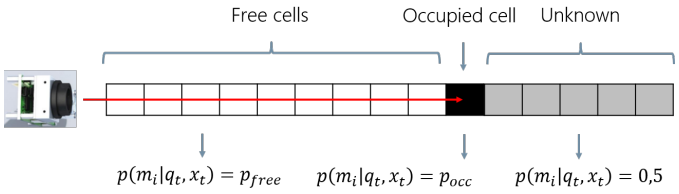

Fig. 2. Inverse Sensor Model

Figure 2 represents the basic idea of the *inverse sensor model* for our Solid State LiDAR. The sensor measurement (red arrow) pierces all the free (white) cells up to the occupied (black) one. Considering only the current observation, nothing can be stated on the (grey) cells which are not interested by the measurement. Hence, $p(m_i|q_t, x_t)$ is set to p_{free} for the white cells, to p_{occ} for the black one and 0.5 for the grey ones, respectively. Different extensions of this formulation are presented in the literature: in Sabatini et al. (2018) the mapping accuracy obtained with the presented method is improved by superimposing a small oscillation to the robot motion; in Thrun (2003) the so called *forward sensor model* is exploited to solve the

mapping problem in the original high-dimensional space, thereby maintaining all dependencies between neighboring cells. Moreover, *forward sensor models* describes the physical phenomena that underlie the data generation, from the cause to the measurement. As a result, maps generated by the *forward sensor model* approach are often more accurate than those generated using the traditional technique. Despite its better accuracy, the authors state that this approach is not suitable for real time applications, because the map is generated solving an optimization problem, which can be computationally expensive. Instead, the recursive formulation of (2) allows real time implementation. Furthermore, the final objective of the proposed system is to warn the driver of the presence of an obstacle just to avoid it. For this purpose a extremely detailed map of the environment is not required. Therefore, the *inverse sensor model* formulation will be used.

To apply the standard Occupancy Grid algorithm and to exploit all the available range, the LiDAR sensor should be mounted such that laser beam is parallel to the ground and at a proper height to frame the obstacles of interests. However, the snow groomer is equipped with a front blade. The blade is 1.2 meters tall and prevents the installation of any forward looking sensor. The LiDAR is thus installed on the top of the cabin, $h = 3.1$ meters above the ground, with a mounting angle α with respect to the vertical axis. Figure 3 illustrates the top and the lateral views of the laser beam. The sensor is centered with respect to the cabin and each sector k looks at a different portion of the environment in front of the vehicle. γ_k is the angle with respect to the longitudinal axis of the bisector of the k^{th} sector. Due to the mounting configuration, the ground

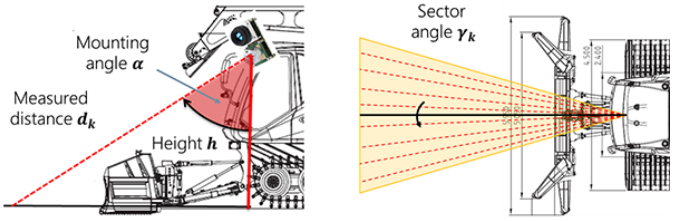

Fig. 3. Top and lateral views of the laser beam

is always involved in the measurement. Consequently, the standard approach would always consider the ground as an obstacle.

4. PROPOSED APPROACH

In this Section a novel *inverse sensor model* for the LiDAR sensor is discussed. The algorithm considers the mounting configuration and the angular resolution of the sensor.

4.1 Inverse Sensor Model

Ski slopes conformation is predominantly a regular flat surface. The main task of snow groomers is to smooth out any surface unevenness caused by the skiers during the day or precipitation or wind. The front blade pushes snow ahead of it and then it is flattened by the tiller installed in the back. The result is a flat and uniform surface with the characteristic corduroy pattern.

The proposed approach assumes that the vehicle moves on a locally constant-grade surface and that the road grade variations have a longer wave length than the FOV of the sensors. In this scenario, it is possible to calculate the height z of the object's portion framed by the laser beam, through the triangulation of the measured distance and the information of the mounting configuration. This idea can be modelled through the *inverse sensor model* illustrated in Figure 4, where the occupancy probability of the involved cells is a function of the expected height. The taller the obstacle, the higher the probability that the current cell is occupied. This concept can be modeled in

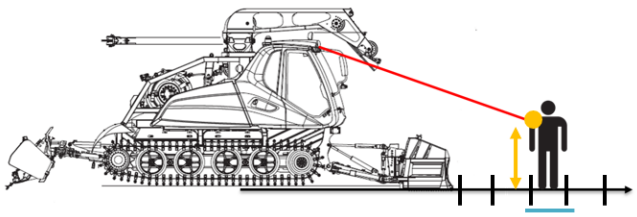

Fig. 4. Basic idea of the probability height correspondence.

the probabilistic framework as:

$$p(m_i|q_t, x_t) = \begin{cases} p_{free} & z_t \leqslant z_{min} \\ p_{free} + \dfrac{p_{occ} - p_{free}}{z_{max} - z_{min}} z_t & z_{min} < z_t \leqslant z_{max} \\ p_{occ} & z_t > z_{max} \end{cases} \quad (3)$$

where z_{min}, z_{max}, p_{free}, p_{occ} are user defined parameters (see Figure 5). The proposed *inverse sensor model* can be tuned depending on the current application.

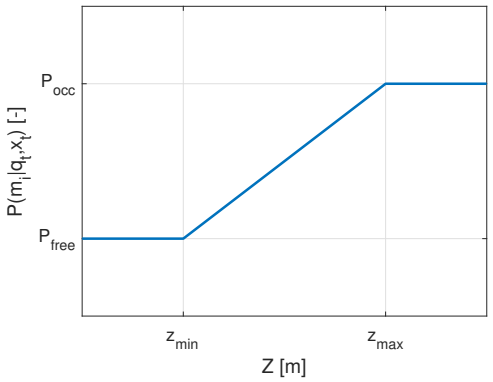

Fig. 5. Inverse Sensor Model

To determine which cells are involved by the current measurement, we have to deal with the angular resolution of the sensor. Figure 6 shows an illustration of this phenomenon. Point A causes the range measurement d_k, and only the grey colored cell should be considered. However it is not possible to determine the location and the size of the obstacle inside the sector area. To overcome this issue, the following approach is proposed: the measured distance d_k by the k^{th} sector is arbitrarily assigned to the bisector (point B). Then, the occupancy probability of all the cells along the sector width w_k is updated (see the

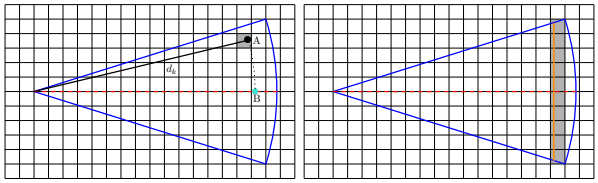

Fig. 6. Representation of the Sector measurement model for a single segment.

right plot of Figure 6). The sector width w_k, related to the measurement d_k, can be calculated as:

$$w_k(d_k, \alpha, FOV) = 2d_k \sin(\alpha) \tan\left(\frac{FOV}{16}\right)$$

Note that the higher is the measured distance, the higher is the amount of cells interested by the current measurement.

4.2 Algorithm

In order to create a 2D map, two reference frames are defined: the *global reference frame* and the *snow groomer reference frame* that describes the pose of the sensor inside the global map (see Figure 7). At each iteration the 2D

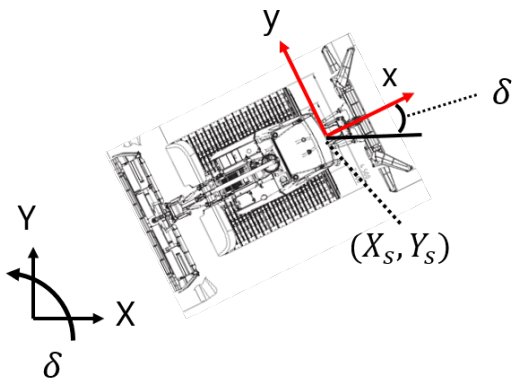

Fig. 7. Snow Groomer frame and Global Reference frame

Occupancy Grid is updated with the following steps:

(1) The longitudinal speed V_x and the yaw rate ω_z are integrated to update the position of the *snow groomer reference frame*:

$$X_{S_{t+1}} = X_{S_t} + \Delta_t V_{x_t} \cos(\delta_t)$$
$$Y_{S_{t+1}} = Y_{S_t} + \Delta_t V_{x_t} \sin(\delta_t)$$
$$\delta_{t+1} = \delta_t + \Delta_t \omega_{z_t}$$

where Δ_t is the sampling time.

(2) The measurement of each sector k is defined in the *snow groomer reference frame* as:

$$x_{k_t} = d_{k_t} \sin(\alpha) \cos(\gamma_k)$$
$$y_{k_t} = d_{k_t} \sin(\alpha) \sin(\gamma_k)$$
$$z_{k_t} = h - d_{k_t} \cos(\alpha)$$

(3) Then they are projected in the *global reference frame* as:

$$\begin{bmatrix} X_{k_t} \\ Y_{k_t} \end{bmatrix} = \begin{bmatrix} \cos(\delta_t) & -\sin(\delta_t) \\ \sin(\delta_t) & \cos(\delta_t) \end{bmatrix} \begin{bmatrix} x_{k_t} \\ y_{k_t} \end{bmatrix} + \begin{bmatrix} X_{S_t} \\ Y_{S_t} \end{bmatrix}$$

(4) The x_k and y_k components are used to identify the cells m_i interested in the current iteration. Their probability value is updated according to (2), where the probability $p(m_i|q_t, x_t)$ is calculated according to the presented *inverse sensor model*.

5. EXPERIMENTAL RESULTS

In this Section, the performance of the proposed obstacle-detection system is discussed through experimental data. The data are collected in Stelvio Pass (Italy). This work focuses on the detection of a person in 3 different position: standing, crouched and laying down on the snow.

Firstly, the detection region of the LiDAR sensor is experimentally evaluated: the vehicle is still on a flat and regular surface, while a moving target, actually a person, moves in the front area. In this way the detection region is pointwise determined. Figure 8 shows the top view of the detection region for different mounting angles α. The sensor is located in the origin and the black line represents the front blade. This analysis shows how even a

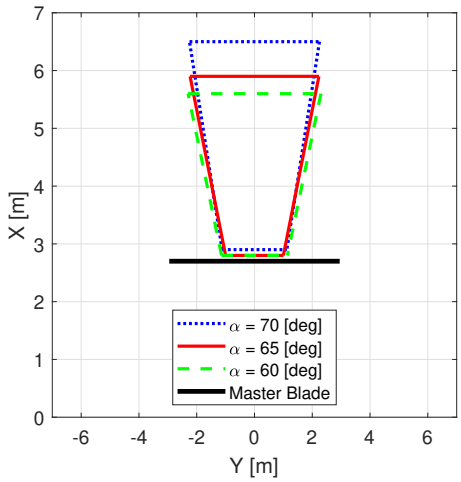

Fig. 8. Detection region of the LiDAR sensor for different mounting angles. The black line represents the front blade.

small variation of the mounting angle affects the detection region. The effects of the mounting angle uncertainty is further analysed in the dynamic tests. The following tests refer to a mounting angle $\alpha = 70$ degrees.

The test protocol is the following:

- The snow groomer is still without any obstacle in the front.
- The vehicle accelerates and reaches the nominal speed of $4[m/s]$.
- The vehicle stops when the target is 20 centimeters from the front blade.

Figure 9, Figure 10 and Figure 11 show the longitudinal speed of the snow groomer, the raw measurements of the LiDAR sensor and the expected height of the obstacle, for the first, second and third configurations, respectively. Since the tests do not include turnings, the vehicle yaw rate is omitted in the analysis. In all the tests, even if there is no obstacle in front of the vehicle, the expected height: assumes values different from zero when the vehicle is still and is affected by measurement noise when the vehicle is in motion. This is due to the unevenness of the ground:

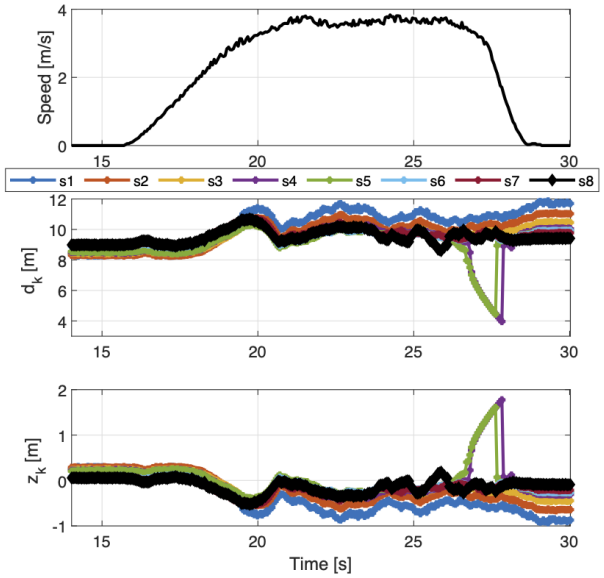

Fig. 9. Test with a standing person as obstacle

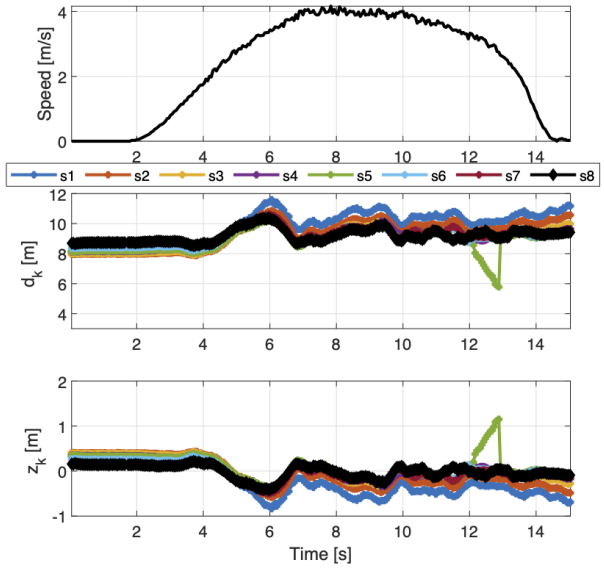

Fig. 10. Test with a crouched person as obstacle

- the sensor is pointing to the fresh snow (*i.e.* an irregular surface).
- the vehicle drives over an irregular surface and its pitch dynamics is excited. This changes the pose of the sensor with respect to the ground.

As a result, the calculation of the obstacle height is affected.

The standard deviation of the noise is respectively 5 centimeters at zero speed. This value is comparable with the LiDAR sensor accuracy. While, during the motion, the standard deviation of the noise is 30 centimeters.

The videos confirm that the peaks in Figure 9 and Figure 10 of the measured distance by sectors 4 and 5, are due

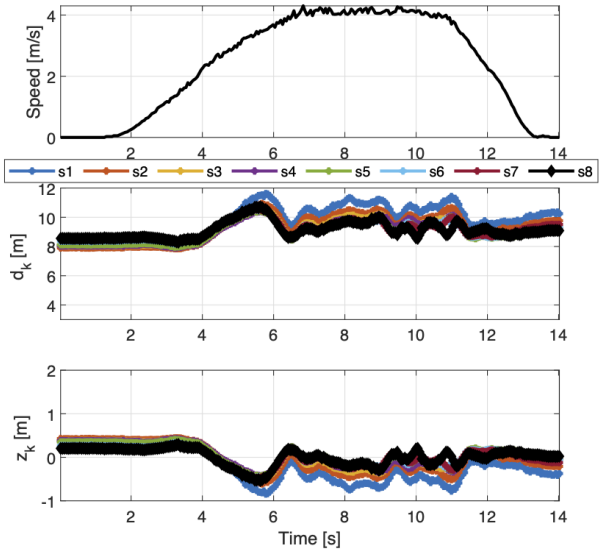

Fig. 11. Test with a laying down person as obstacle

to the person. The calculated height of the obstacles are respectively 1.74 and 1.12 meters for the standing and the crouched configurations. These values are consistent with the real height of the targets.

However, in the laying down test there is no visible variation of the measured distance and consequently of the expected height. The reasons for this result are twofold: the person laying down on the snow is not taller than the ground irregularities; the amplitude of measurement noise is comparable with the height of the obstacle. Applying the proposed approach, it is possible to obtain the Occupancy Grid of the surrounding environment, where at each iteration a portion of the map is updated. Each cell is a 20 centimeters side square, while the inverse sensor model parameters are set as $z_{min} = 0.2\,[m]$, $z_{max} = 1\,[m]$, $p_{free} = 0.3$, $p_{occ} = 0.9$. Figure 12 presents the Occupancy Grids obtained at the end of the tests, where:

- the grey cells represent the part of the map which is not interested by the sensor measurements, hence their probability is still $0,5$.
- the white cells represent the obstacle-free part of the map .
- the black cells represent the detected obstacles.

According to the previous analysis, the system can detect the person in both standing and crouched positions, where the dimensions of the resulting obstacles on the Occupancy Map are $(1.6, 0.4)$ and $(1, 0.4)$ meters respectively. Moreover, right after the location of the detected obstacle, there is an unknown (grey) area which is not reached by the laser beam.

The person is detected when it is 3 meters far from the front blade for both configurations, hence the proposed system could avoid possible accidents. However, the system can not detect a person laying down on the ground. An additional sensor is then required: an infrared camera, for example, could detect the laying down person, thanks to the temperature difference between the body and the snow.

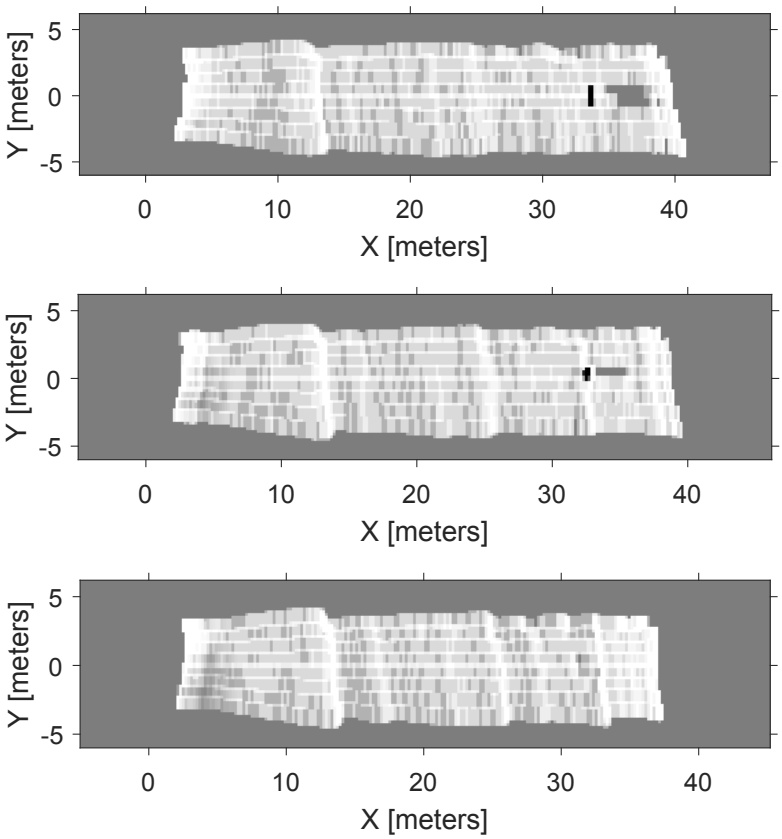

Fig. 12. Occupancy Grids: standing test (first plot), crouched test (second plot) and laying down test (third plot).

6. CONCLUSIONS

This paper presents an obstacle-detection system for snow groomers based on the measurements of a 2D solid-state LiDAR. The algorithm builds an Occupancy Grid of the surrounding environment. The occupancy probability is updated in function of the expected height of the framed obstacle. The angular resolution of the LiDAR sensor is accounted in the inverse sensor model. Experimental results show how the system can detect a standing and a crouched person.

7. ACKNOWLEDGMENTS

The authors thank Prinoth S.p.A. for providing the test vehicle.

REFERENCES

Broggi, A. and Fascioli, A. (2002). Artificial vision in extreme environments for snowcat tracks detection. *IEEE Transactions on Intelligent Transportation Systems*, 3(3), 162–172.

Corno, M., Roselli, F., Onesto, L., Molinaro, F., Graves, E., Doubek, A., and Savaresi, S. (2018). Experimental validation of an antilock braking system for snowmobiles with lateral stability considerations. *IEEE Transactions on Control Systems Technology*, 1–8.

Elfes, A. (1989). Using occupancy grids for mobile robot perception and navigation. *Computer*, 22(6), 46–57.

Gustafsson, T. and Eriksson, A. (2013). Off-road vehicle fatalities: A comparison of all-terrain vehicle and snowmobile accidents in sweden. *IATSS research*, 37(1), 12–15.

Kukko, A., Anttila, K., Manninen, T., Kaasalainen, S., and Kaartinen, H. (2013). Snow surface roughness from mobile laser scanning data. *Cold Regions Science and Technology*, 96, 23–35.

Leddartech (2019). https://leddartech.com/lidar/leddar-vu8-solid-state-lidar-sensor-module/.

Sabatini, S., Corno, M., Fiorenti, S., and Savaresi, S.M. (2018). Improving occupancy grid mapping via dithering for a mobile robot equipped with solid-state lidar sensors. In *2018 IEEE Conference on Control Technology and Applications (CCTA)*, 1145–1150. IEEE.

Thrun, S. (2003). Learning occupancy grid maps with forward sensor models. *Autonomous robots*, 15(2), 111–127.

Thrun, S., Burgard, W., and Fox, D. (2005). *Probabilistic robotics*. MIT press.

Vanlaar, W., McAteer, H., Brown, S., Crain, J., McFaull, S., and Hing, M.M. (2015). Injuries related to off-road vehicles in canada. *Accident Analysis & Prevention*, 75, 264–271.

Yanchar, N.L., Society, C.P., and Committee, I.P. (2012). Preventing injuries from all-terrain vehicles. *Paediatrics & child health*, 17(7), NP–NP.

Ziebinski, A., Cupek, R., Erdogan, H., and Waechter, S. (2016). A survey of adas technologies for the future perspective of sensor fusion. In *International Conference on Computational Collective Intelligence*, 135–146. Springer.